JOURNAL OF THERMOPHYSICS AND HEAT TRANSFER
Vol. 6, No. 4, Oct.–Dec. 1992

# Effect of Free Surface Shape on Combined Thermocapillary and Natural Convection

Yasuhiro Kamotani*
*Case Western Reserve University, Cleveland, Ohio 44106*
and
Jonathan Platt†
*NASA Lewis Research Center, Cleveland, Ohio 44135*

**Combined thermocapillary and natural convection in an open square cavity with differentially-heated side walls is studied numerically as well as experimentally. The test fluid is silicone oil with Prandtl number of 105. The shape of fluid-free surface is made either flat or curved to study its effect on the flow. A finite difference scheme to deal with a curved free surface is developed. The experimental results shown agree with the numerical results. With the curved-free surface, the flow and local heat transfer rate are reduced in the corner regions, and a sharp peak in heat transfer rate at the top edge of the cold wall disappears.**

## Nomenclature

$\underline{Bo}$ = static Bond number, $\rho g L^2 \sigma$
$Bo$ = dynamic Bond number, $Gr/R\sigma$
$Gr$ = Grashof number, $g\beta\Delta T L^3/\nu^2$
$g$ = gravitational acceleration
$h$ = free surface height
$L$ = container dimension
$Nu$ = local Nusselt number, Eq. (14)
$Pr$ = Prandtl number
$R_\sigma$ = surface tension Reynolds number, $\sigma_T \Delta T L/\mu\nu$
$T$ = temperature nondimensionalized as $(T - T_c)/\Delta T$
$T_c$ = cold wall temperature
$(u, v)$ = velocity in $(x, y)$ domain nondimensionalized by $\nu/L$
$(x, y)$ = coordinate system, (Fig. 1)
$\beta$ = volumetric expansion coefficient in $Gr$
$\Delta T$ = temperature difference between hot and cold wall
$\mu$ = viscosity
$\nu$ = kinematic viscosity
$(\xi, \eta)$ = coordinates, Eq. (1)
$\rho$ = density
$\sigma$ = surface tension
$\sigma_T$ = temperature coefficient of surface tension
$\tau$ = shear stress at free surface
$\phi$ = inclination angle of free surface
$\psi$ = stream function
$\omega$ = vorticity

## Introduction

THE flow caused by heat-induced surface tension variation along a liquid-free surface is called thermocapillary flow. In a 1 $g$ environment the flow coexists with buoyancy driven flow and is usually overshadowed by it (except for flows of small dimension) but in a low $g$ environment thermocapillary effects could dominate. The attractiveness of the low $g$ space environment for crystal growth stems from the belief that crystal imperfections and impurities can be reduced by minimizing natural convection and utilizing containerless crystal growth process (e.g., float zone growth). Because liquid-free surfaces with temperature gradients are inherent to all containerless processes, convection effects associated with thermocapillary flows could be important in space.[1,2]

Thermocapillary flow and combined thermocapillary and buoyant flow have been studied in the past by several investigators. The work pertinent to the present study are the numerical computations discussed in Refs. 3–6 and the experimental work in Ref. 7. All the numerical work considered flow in a square cavity with differentially-heated side walls and with a flat undeformable free surface. The effects of various dimensionless parameters on the velocity and temperature fields were investigated. Some important numerical problems in analyzing high Marangoni number thermocapillary flow are discussed by Chen.[8] Metzger and Schwabe[7] used a square cavity with a flat-free surface in their experiment and studied the interaction between thermocapillary and buoyant flow under various heating conditions.

Although a flat-free surface simplifies the analyses, the free surface can be quite curved in low $g$ and 1 $g$ situations where thermocapillary flow is important. Cuvelier and Driessen[9] numerically analyzed steady thermocapillary and buoyant flow in a cavity with a deformable-free surface using a finite element method. They studied the effect of various parameters on the free surface shape and flowfield and showed that the flow can cause a large free surface deformation under some conditions, but in reality, those conditions require unrealistic physical properties. Neitzel et al.[10] employed a similar finite element method to study thermocapillary and buoyant convection in model float zones of $NaNO_3$ and Si. They noted that within the parametric ranges studied the flow-induced free surface deformation was very small. Thermocapillary flow in a cavity with a curved but fixed-free surface using finite difference methods was investigated.[11,12] Kamotani[11] employed the vorticity-stream function formulation and showed the effect of highly curved-free surface shape on the flow and heat transfer for high and low $Pr$ fluids. Keller and Bergman[12] used a method based on the primitive variables and analyzed the effect of convex- and concave-free surface shape for a unit $Pr$ fluid. They did not get convergence beyond the Marangoni number $10^3$ and the results are presented only for mildly curved surfaces ($\theta$ larger than 55 deg).

In the present work, based on the work by Kamotani,[11] combined thermocapillary and buoyancy flow is analyzed with a curved- but fixed-free surface. An experiment is also conducted to check the accuracy of the prediction. The effect of

Received May 15, 1991; revision received Oct. 15, 1991; accepted for publication Oct. 25, 1991. 

*Professor, Department of Mechanical and Aerospace Engineering, Associate Fellow AIAA.
†Aerospace Engineer, Microgravity Fluid Branch, Space Experiment Division.

a highly-curved surface thermocapillary flow in microgravity is also discussed.

## Problem Formulation

Consider a two-dimensional square cavity of dimension $L$, partially filled with a liquid (Fig. 1) that has a line of contact with the side walls at the top edges of the cavity. The apparent contact angle $\theta$ must be greater than or equal to the actual contact angle between the liquid and solid in order for the contact line to stay at the edge. In the absence of gravity, the static shape of the free surface has a constant radius of curvature, but when gravity is present the surface takes on a more complicated shape determined by the $Bo$ and $\theta$.

When the side wall temperatures are fixed to impose a horizontal temperature difference $\Delta T$ across the container (with the free surface and bottom wall considered thermally insulated), flow develops due to surface tension variations (thermocapillary flow) and, in the presence of gravity, due to density gradients (buoyant flow). The capillary number, a dimensionless parameter representing the ratio of viscous-to-surface tension forces, is a measure of free surface deformation caused by the flow. Because the capillary number is much less than unity in the present experiment (as discussed below), the free surface is assumed in the present analysis to maintain its static shape.

## Numerical Analysis

Laminar, two-dimensional, steady flow is analyzed. The present numerical scheme is based on one developed[13,14] to analyze flow about arbitrary two-dimensional bodies. Because the present scheme is discussed in Kamotani,[11] it is only outlined here.

The body-fitted curvilinear coordinates are adopted. They are generated from the original Cartesian coordinates $(x, y)$ (defined in Fig. 1) by the following transformation:

$$\xi = x \quad \text{and} \quad \eta = y/h(x) \tag{1}$$

where $h(x)$ represents the $y$-coordinates of the free surface. Thus $\xi = 0$ and $\xi = 1$ correspond to the hot and cold walls, respectively, and $\eta = 0$ and $\eta = 1$ correspond to the bottom and the free surface, respectively. The curvilinear coordinates in the $(x, y)$ plane and those in $(\xi, \eta)$ plane are illustrated in Fig. 1.

The present numerical scheme is based on the vorticity-stream function formulation. The dimensionles vorticity, stream function, and energy equations in the transformed plane can be written as

$$\omega_t + (\psi_\eta\omega_\xi - \psi_\xi\omega_\eta)/J = Q\omega_\eta + (\alpha\omega_{\xi\xi} - 2\beta\omega_{\xi\eta} + \gamma\omega_{\eta\eta})/J^2 + Gr(y_\eta T_\xi - y_\xi T\eta) \tag{2}$$

$$\omega = -(\alpha\psi_{\xi\xi} - 2\beta\psi_{\xi\eta} + \gamma\psi_{\eta\eta})/J^2 - Q\psi_\eta \tag{3}$$

$$T_t + (\psi_\eta T_\xi - \psi_\xi T_\eta)/J^2 = QT_\eta/Pr + (\alpha T_{\xi\xi} - 2\beta T_{\xi\eta} + \gamma T_{\eta\eta})/(PrJ^2) \tag{4}$$

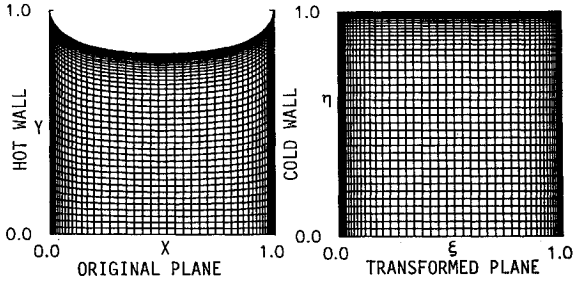


**Fig. 1 Original curved surface domain and transformed domain.**

with

$$\alpha = h^2$$
$$\beta = hh_x\eta$$
$$\gamma = 1 + (h_x\eta)^2 \tag{5}$$
$$J = h$$
$$Q = \eta(2h_x^2 - hh_{xx})/h^2$$

In the above equation lengths, time $t$, vorticity $\omega$, and stream function $\psi$ are dimensionless with respect to $L$, $L^2/\nu$, $\nu/L^2$, and $\nu$, respectively. Temperature $T$ is made dimensionless as $(T - T_c)/\Delta T$.

The boundary conditions along the solid surface are

$$\psi(0, \eta) = \psi(1, \eta) = \psi(\xi, 0) = 0$$
$$T(0, \eta) = 1, \quad T(1, \eta) = T_\eta(\xi, 0) = 0$$
$$\omega(0, \eta) = -\psi_{\xi\xi}(0, \eta), \quad \omega(1, \eta) = -\psi_{\xi\xi}(1, \eta) \tag{6}$$
$$\omega(\xi, 0) = -\psi_{\eta\eta}(\xi, 0)/h^2$$

The temperature and stream function boundary conditions along the free surface are

$$\psi(\xi, 1) = 0 \quad \text{and} \quad T_n(\xi, 1) = 0 \tag{7}$$

where $n$ denotes the direction normal to the free surface.

The vorticity boundary condition at the free surface is more complex. An approximate condition was used in Kamotani[11] but the exact condition can be derived as follows. The tangential stress at the free surface can be expressed as

$$\tau/\mu = (\cos^2\phi - \sin^2\phi)(u_y + v_x) - 4\sin\phi\cos\phi v_x \tag{8}$$

where $\phi$ is the angle the free surface makes with the horizontal, $u$ and $v$ are velocity components in the $(x, y)$ plane. With the help of the impermeability condition ($v = u\tan\phi$) and the continuity equation ($u_x + v_y = 0$), Eq. (8) can be reduced to

$$\tau/\mu = u_y - v_x + 2u\phi_x = -\omega + 2u\phi_x (\phi \neq \pi/2) \tag{9}$$

For thermocapillary flow the boundary condition at the free surface is

$$\tau = -\sigma_T T_s \tag{10}$$

where $s$ denotes the direction tangent to the free surface. From Eqs. (9) and (10) one gets

$$\omega = \sigma_T T_s/\mu + 2u\phi_x$$

or in terms of the dimensionless variables

$$\omega = T_\sigma T_s + 2u\phi_x \tag{11}$$

at the free surface.

In 0 $g$ the free surface shape is a circular arc with angle $\phi$ between its tangent and the side wall at the contact line. In 1 $g$ the shape is determined by the balance between surface tension and gravity, which can be written in dimensionless form as

$$Boh = h_{xx}/(1 + h_x^2)^{3/2} \tag{12}$$

The above equation is solved with the boundary conditions

$$h_x(0) = -\cot\phi \quad \text{and} \quad h_x(1) = \cot\phi \tag{13}$$

The equations and boundary conditions describing the flow contain four dimensionless parameters 1) $Gr$; 2) $R_\sigma$; 3) $Pr$; and 4) $Bo$. The ratio of buoyancy to thermocapillary forces is represented by $\overline{Bo} = Gr/R_\sigma$.

A finite difference method is used to solve the problem. The time derivatives are forward-differenced and the convection terms are finite-differenced based on a first-order upwind-differencing scheme. The remaining terms are approximated by second-order central difference expressions. For convenience a time-derivative term is added to the stream function equation. Then the time-dependent solutions are obtained for the vorticity, energy, and stream function equations using the ADI method. The solutions are considered converged when the largest relative variation in any of $\omega$, $T$, and $\psi$ is less than $10^{-4}$. The grid system adopted herein will be discussed below.

The heat transfer rate at the vertical walls is represented by the local $Nu$:

$$Nu = \partial T/\partial x \quad \text{at} \quad x = 0, 1 \tag{14}$$

In the case of a thermally insulated concave free surface $Nu$ is theoretically zero at $y = 1$ and has a finite value when the surface is flat.

## Description of Experiment

An experiment was conducted to test the results of the numerical analysis. The test section used was an open rectangular box with copper side walls (that were maintained at constant temperatures by running constant temperature water through them), two plexiglas end walls, and a plexiglas bottom. It had a small cross section (1 cm × 1 cm) and relatively large width (5 cm) to produce approximately two-dimensional flow. The test fluid was silicone oil with 10-cS kinematic viscosity at 25°C.

A microscopic observation of the fluid meniscus showed that the contact angle between the test fluid and the copper wall in air is about 5–10 deg. An apparent contact angle of 90 deg (flat-free surface) was obtained by filling the test section to the rim of the container. The curved-free surface was obtained by withdrawing fluid from the filled container until the contact line started to move downward. The curved-free surface shape is drawn in Fig. 1. The shape could be made more curved by using a smaller test cell but that would make it more difficult to measure the temperature field in detail.

Temperature data was taken by three thermocouples: two imbedded in the copper side walls to measure the wall temperatures and one mounted on a movable traverse to measure temperatures in the fluid. The diameter of the latter thermocouple joint was 0.038 mm, that was small enough to measure temperatures close to the fluid-free surface yet strong enough to maintain its position against the flow. According to the numerical analysis the thinnest thermal boundary-layer thickness to be resolved in the experiment was about 0.25 mm. To measure the temperature of the free surface accurately was not an easy task but in similar experiments (e.g., Kamotani and Lee[15]) we have established a procedure for the measurement.

The temperature probe was bent in such a way that it touched the free surface almost horizontally from the direction normal to the $x$-$y$ plane to minimize the measurement error due to heat conduction through the wire leads. With the help of a microscope the probe was positions so that the tip of the thermocouple junction was seen to create a tiny hump at the surface. In addition, the hot and cold wall temperatures were adjusted to make the average surface temperature close to the surrounding air temperature. The error in the surface temperature measurement is estimated to be within ±5% of imposed $\Delta T$. The imposed horizontal temperature difference was 10 ± 0.1°C, a value large enough to allow accurate measurement of temperature distribution yet still small enough for the assumption of constant viscosity to be approximately valid (viscosity variation was ±8% in the container).

Fluid motion was visualized by adding small (1–10 μm diam) alumina particles to the fluid. A HeNe laser light sheet created by a cylindrical lens illuminated the center plane of the cavity to allow the flow to be photographed. A 35-mm camera with a magnifying lens system was used.

For the experiment described above the values of the dimensionless parameters are: $Gr = 1130$, $R_\sigma = 67$, and $Pr = 105$. $\overline{Bo} = 17$ and thus buoyancy forces are greater than surface tension forces in driving the flow as a whole ($Bo = 45$).

## Results and Discussion

### Grid System for Numerical Analysis

Based on the past numerical analyses of thermocapillary flow and combined thermocapillary and buoyant flow, a nonuniform grid system was adopted with meshes graded toward the hot and cold walls and toward the free surface. To check the influence of the grid on the solution, various systems were tested under the conditions of the experiment. The velocity and temperature distributions at the free surface computed with three different grids are shown in Fig. 2 for both flat and curved surface shapes. The coarse 25 × 22 (horizontal by vertical) grid with the smallest mesh size of 0.01 was not adequate for the flat surface case. The 46 × 40 grid with the smallest spacing of 0.005 was considered to be acceptable for both cases. The computed $Nu$ were 6.00 (37 × 31) and 6.01 (46 × 40) for the flat surface and 5.26 (37 × 31) and 5.23 (46 × 40) for the curved surface.

For the flat surface case the surface velocity distribution has a spike near the cold wall due to thermocapillary flow driven by a sharp temperature gradient in that region (Fig. 2a). As discussed by Chen,[8] an accurate numerical scheme with a very fine grid system is needed to resolve the cold corner region accurately at high $Ma$. At $Ma = 7.0 \times 10^3$ in the present work the corner region is not accurately resolved by 46 × 40 system and the peak value would increase with a finer grid. An extrapolation of the result by Zehr et al.[4] shows that the peak value is about 0.07 (in their units) at $Ma = 7 \times 10^3$ while the present computation done for pure ther-

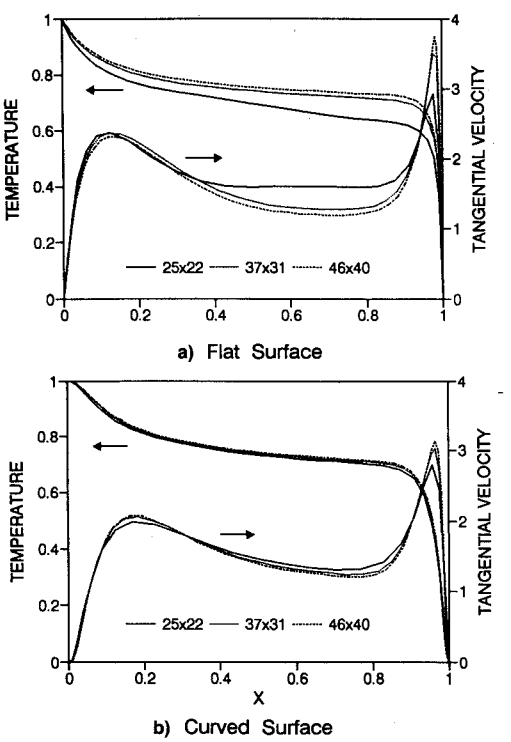


**Fig. 2 Surface velocity and temperature distributions computed with various grid systems ($Gr = 1130$, $R_\sigma = 67$, $Pr = 105$).**

mocapillary flow with the 46 × 40 grid gives the value of 0.052 using the same units. Based on the scaling analysis of Hu[16] for thermocapillary flow, it can be shown that the extent of the corner region from the cold wall scales with $Ma^{-1}$ when $Pr \geq 1$, which is a relatively small region when $Ma$ is large. Therefore, the overall flow structure and temperature field are not influenced by the corner region flow, that agrees with the result by Zebib et al.[3] in which the values of $Nu$, maximum stream function, and maximum vorticity are shown to scale with the bulk flow parameters. We computed the cases studied[3] using the 46 × 40 grid and found that the computed values of $Nu$ and $\psi_{max}$ were all within ±2% of the values given as long as $Ma$ and $Ra$ were less than $10^4$. In comparison, in the case of the curved-free surface, the corner resolution problem is less severe because the surface temperature variation is more gradual so that the peak appears at a larger distance from the cold wall (Fig. 2b).

In the numerical analysis[12] the surface velocity distribution computed at $Ma = 10^3$ for the 0 $g$ free surface shape with $\theta = 56$ deg is shown to depend very strongly on the grid used (the results with 20 × 20, 40 × 40, and 80 × 60 nonuniform grids are shown). Moreover, the velocity spike in the cold corner disappears with the finest grid. We analyzed the same problem using the present method with 25 × 22, 37 × 31, and 46 × 40 grids and found that the grid influence on the surface velocity distribution was similar to the one shown in Fig. 2b and that a velocity spike in the cold corner region was not greatly influenced by the grid system.

To check the influence of the flow on the free surface, capillary number that is defined as $\mu u/\sigma$, is computed based on the velocity in Fig. 2 and the experimental conditions. The value is no more than $10^{-3}$, that is small enough to justify the assumption of negligible free-surface deformation due to fluid motion.

### Numerical and Experimental Results

The photos of flow patterns for flat and curved-free surfaces are shown in Fig. 3. The left side wall is hot, so the fluid moves from left to right along the free surface. Since the surface tension of silicone oil decreases with increasing temperature, the thermocapillary driving force augments the buoyant flow along the surface. In both cases the flow pattern is predominantly unicellular with relatively weak bicellular motion in the upper half. The center of the left cell is located higher than the right cell. The numerically predicted streamline patterns for the corresponding cases are also presented in Fig. 3 for comparison. The experimental and computed results agree in terms of the overall flow pattern and the location of the closed cells. In order to see the separate influence of buoyancy and thermocapillarity, purely thermocapillary flow and purely buoyant flow with zero shear along the free surface are computed and the steamlines are plotted in Fig. 4. In the case of thermocapillary flow (Fig. 4a) the flow structure is unicellular without secondary cells. As discussed above, the flow goes deep into the top cold corner region but the volume flux going into the corner is relatively small. In pure buoyant flow (Fig. 4b) there are two closed cells as in the combined case; the location of the left cell is now slightly lower than the right one without the thermocapillary driving force in the top left corner. The $Bo = 17$ in the present experiment indicates relatively strong buoyant flow, but locally thermocapillarity has an appreciable effect on the flow as seen above.

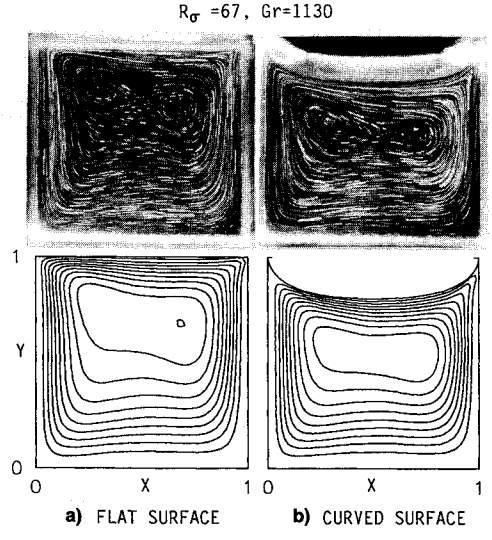


**Fig. 3 Measured and computed streamlines.**

Figure 5 shows the computed velocity distributions at $x/L = 0.5$. The $y$-coordinate is nondimensionalized by the fluid depth at $x/L = 0.5$. As seen in the figure, the influence of thermocapillary increases the velocity near the free surface and also decreases the surface flow region (the region with positive $u$ velocity). If the $y$-coordinate is adjusted as shown, the velocity profile is slightly altered by the curved free surface around $x/L = 0.5$. In Figs. 2a and 2b it is clear that in the curved surface case the velocity in the corner region, especially near the hot wall, is reduced because of the meniscus shape.

The measured and computed surface temperature distributions for flat and curved surfaces are shown in Fig. 6; the computation and the data agree. The curved meniscus does not change the distribution greatly, although it should be noted that the distribution is plotted against $x$ and not as a function of distance along the free surface. The surface temperature near the hot wall is slightly higher in the curved meniscus case because the curved meniscus results in decreased convection; along the rest of the surface the temperature is slightly lower when the meniscus is curved.

Temperature distributions in the bulk fluid are measured at three different $x$ locations and compared with the numerical results in Fig. 7. They agree, except at $x/L = 0.15$ where the fluid temperature is higher than predicted, especially near the

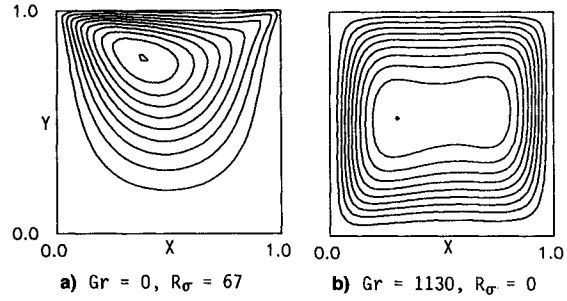


**Fig. 4 Computed streamlines for pure thermocapillary and pure buoyant flow.**

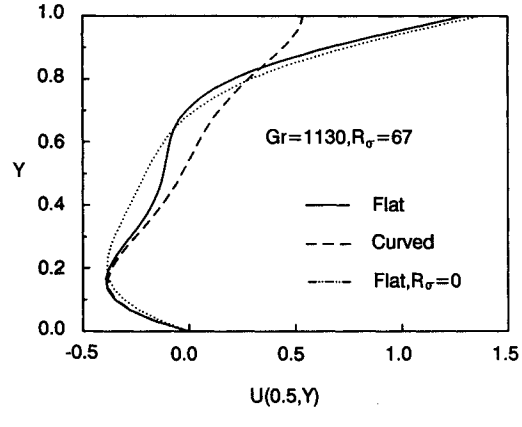


**Fig. 5 Velocity distributions at $x/L = 0.5$ computed for various conditions.**

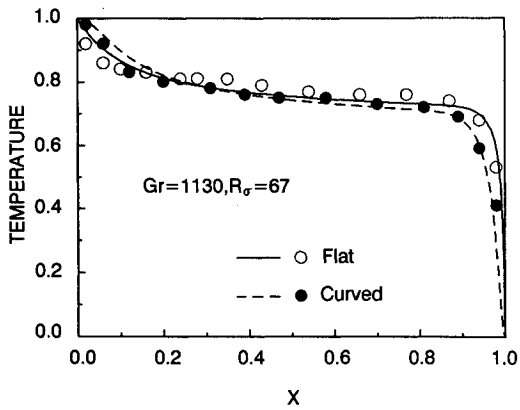


**Fig. 6 Comparison of computed and measured surface temperature distributions.**

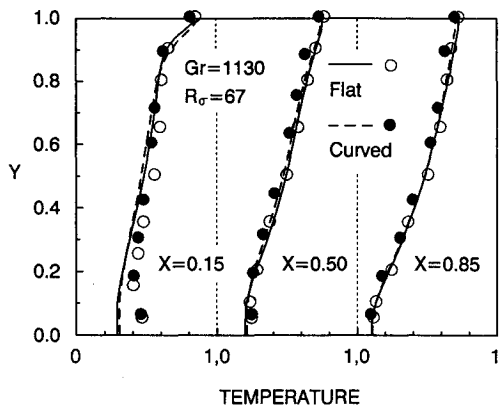


**Fig. 7 Comparison of computed and measured interior temperature distributions.**

bottom wall. The reason for this is that in the experiment the bottom wall is heated by the hot wall through conduction, whereas in the numerical analysis the bottom wall is assumed to be thermally isolated from the hot wall.

The local heat transfer coefficient along the hot and cold walls is shown in Fig. 8. The figure shows the distribution along the top half of the walls because the effect of curved free surface is greatest there. The heat transfer is substantially reduced along the hot wall in the curved surface case due to decreased convection in the top corner. Without thermocapillarity, the heat transfer is also reduced in the hot corner, again showing that the effect of thermocapillary flow is not small in the present experiment. As discussed above, there exists a strong corner flow near the cold wall. In the flat surface case the corner flow impinges directly on the cold wall, resulting in a sharp increase in the heat transfer rate (the maximum *Nu* at the top edge is 63.2, although the value may contain a certain error due to the aforementioned resolution problem). In comparison, since the flow passage is narrower in the cold corner with the curved free surface, heat conduction from the cold wall tends to make temperature more uniform (Figs. 2a and 2b) and at the top edge of the wall the heat transfer rate is theoretically zero, which is correctly predicted by the present analysis as seen in Fig. 8. As a result, the heat transfer rate in the cold corner is greatly reduced. Because of this reduction the grid size requirement is less severe than the flat surface case. As shown in Fig. 8, the 46 × 40 grid system is quite adequate for that case.

### Effect of Highly Curved-Free Surface in 0 *g*

In microgravity a liquid-free surface can be highly curved. Kamotani[11] analyzed the effect of various surface shapes on thermocapillary convection. Since the free surface vorticity boundary condition is more accurate in the present analysis, the effect of a highly-curved surface is reanalyzed herein. The

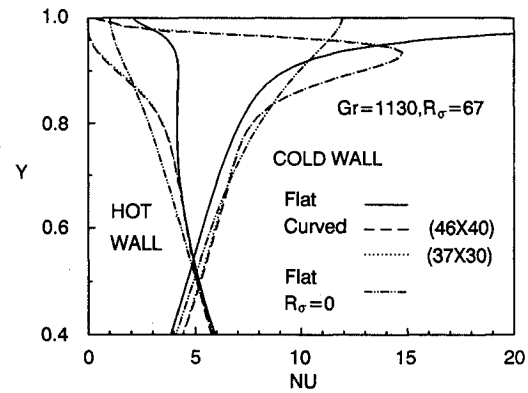


**Fig. 8 Nusselt number distributions computed for various conditions.**

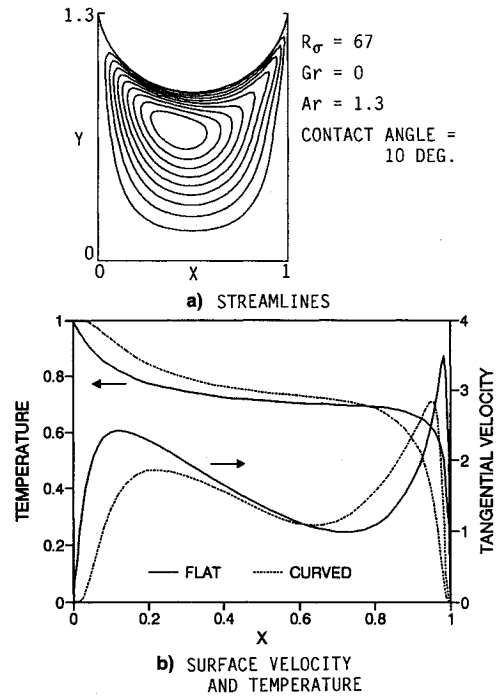


**Fig. 9 Streamlines and surface velocity and temperature distributions with highly curved free surface in 0 *g*.**

contact angle considered is 10 deg, which is less than the smallest value investigated by Kamotani.[11] The result is to be compared with the aforementioned result for the flat surface with $Gr = 0$, so we choose $Pr = 105$ and $R_\sigma = 67$. If the container aspect ratio were kept at 1, the average fluid depth would be greatly reduced by the curved surface; to avoid the effect, the aspect ratio ($Ar$) is increased to 1.3 in the curved case to have the same fluid volume in both cases.

Some important results are presented in Fig. 9. The streamline pattern given in Fig. 9a shows that the flow tends to get into the recessed corner regions but it is nearly stagnant near the contact lines as compared with Fig. 4a. The dimensionless maximum stream function is 0.156 for the flat case and 0.119 for the curved case. Therefore, the overall flow is slower in the curved case despite the fact that the thermocapillary driving force acts over a larger area (the free surface is 42% larger). With the curved surface the thermocapillary force is less effective in driving the unicellular motion because it continuously changes the direction along the surface and also the average driving force is reduced as discussed below. As seen in Fig. 9b, with the curved-free surface the surface temperature becomes more uniform in the hot and cold corners because of reduced convection there. The surface velocity distribution still has two peaks but they are located further away from the walls. The peak values are only slightly reduced by the curved surface. Because the flow is no longer strongly impinging on the top edge of the cold wall, the maximum

heat transfer rate at the cold wall is reduced from $Nu = 53$ for the flat surface, to $Nu = 8.6$ for the curved surface, while the average $Nu$ is reduced from 3.63 to 2.80. As observed by Kamotani,[11] the overall flow quantities are much less influenced by the curved surface than the local quantities in the corner regions.

The computational time increase with an increasingly curved surface. In the present analysis, a time step of $2.0 \times 10^{-6}$ was used for the vorticity equation in the flat surface case, whereas a time step of $10^{-6}$ was used in the highly curved surface case.

## Conclusions

Combined thermocapillary and natural convection in a square cavity with flat and curved-free surfaces is investigated both numerically and experimentally. A numerical scheme is developed to analyze the combined flow with curved-free surfaces and its predictions agree well with the experimental results. The thermocapillary driving force is greatly reduced in the hot and cold corner regions when the free surface is highly curved. Consequently, the flow becomes much slower and the local heat transfer rate is substantially reduced in those regions. When the free surface is flat, thermocapillary flow impinges strongly on the top edge of the cold wall and as a result the heat transfer rate is very large near the edge but the sharp peak disappears when the surface is curved.

## Acknowledgments

The work is supported by NASA Lewis Research Center under NASA Grant NAG 3-570. T. P. Jacobson is the project monitor and R. L. Thompson is the project scientist.

## References

[1]Ostrach, S., "Low-Gravity Fluid Flows," *Annual Review of Fluid Mechanics*, Vol. 14, 1982, pp. 313–345.

[2]Schwabe, D., "Marangoni Effects in Crystal Growth Melts," *PCH PhysicoChemical Hydrodynamics*, Vol. 2, No. 4, 1981, pp. 263–280.

[3]Zebib, A., Homsy, G. M., and Meiburg, E., "High Marangoni Number Convection in a Square Cavity," *Physics of Fluids*, Vol. 28, No. 12, 1989, pp. 3467–3476.

[4]Zehr, R., Chen, M. M., and Mazumder, J., "Thermocapillary Convection of a Differentially Heated Cavity at High Marangoni Numbers," ASME Paper 87-HT-229, Pittsburgh, PA, Aug. 1987.

[5]Bergman, T., and Ramadhyani, S., "Combined Buoyancy- and Thermocapillary-Driven Convection in Open Square Cavities," *Numerical Heat Transfer*, Vol. 9, 1986, pp. 441–451.

[6]Carpenter, B. M., and Homsy, G. M., "Combined Buoyant-Thermocapillary Flow in a Cavity," *Journal of Fluid Mechanics*, Vol. 207, 1989, pp. 121–132.

[7]Metzer, J., and Schwabe, D., "Coupled Buoyant and Thermocapillary Convection," *PCH PhysicoChemical Hydrodynamics*, Vol. 10, No. 3, 1988, pp. 263–282.

[8]Chen, M. M., "Thermocapillary Convection in Materials Processing," *Interdisciplinary Issues in Materials Processing and Manufacturing*, ASME, Vol. 2, 1987, pp. 541–558.

[9]Cuvelier, C., and Driessen, J. M., "Thermocapillary Free Boundaries in Crystal Growth," *Journal of Fluid Mechanics*, Vol. 169, 1986, pp. 1–26.

[10]Neitzel, G. P., Hyer, J. R., and Jankowski, D. F., "Thermocapillary Convection in a Model Float-Zone," AIAA Paper 90-0406, Reno, NV, Jan. 1990.

[11]Kamotani, Y., "Thermocapillary Flow in a Square Cavity with Curved Liquid Free Surface," *Proceedings of AIAA/ASME/SIAM/APS First National Fluid Dynamics Congress*, Cincinnati, OH, July 1988, pp. 1792–1797.

[12]Keller, J. R., and Bergman, T. L., "Thermocapillary Cavity Convection in Wetting and Nonwetting Liquids," *Numerical Heat Transfer*, Vol. 18, Pt. A, 1990, pp. 33–49.

[13]Thompson, J. F., Thames, F. C., and Mastin, C. W., "Automatic Numerical Generation of Body-Fitted Curvilinear Coordinate System for Field Containing Any Number of Arbitrary Two-Dimensional Bodies," *Journal of Computational Physics*, Vol. 19, 1974, pp. 299–319.

[14]Thames, F. C., Thompson, J. F., Mastin, C. W., and Walker, R. L., "Numerical Solutions of Viscous and Potential Flow About Arbitrary Two-Dimensional Bodies Using Body-Fitted Coordinated Systems," *Journal of Computational Physics*, Vol. 24, 1977, pp. 245–273.

[15]Kamotani, Y., and Lee, K. J., "Oscillatory Thermocapillary Flow in a Liquid Column Heated by a Ring Heater," *PCH Physico-Chemical Hydrodynamics*, Vol. 11, Nos. 5 and 6, 1989, pp. 729–736.

[16]Hu, D., "Thermocapillary Flows in an Enclosure of Unit Order Aspect Ratio," Ph.D. Dissertation, Case Western Reserve Univ., Cleveland, OH, 1991.